



# PM<sub>2.5</sub> assimilation within JEDI for NOAA's regional Air Quality Model (AQMv7): application to the September 2020 Western US wildfires

Hongli Wang<sup>1,2</sup>, Cory Martin<sup>3</sup>, Jérôme Barré<sup>4,5</sup>, Ruifang Li<sup>1,2</sup>, Steve Weygandt<sup>2</sup>, Jianping Huang<sup>3</sup>, Youhua Tang<sup>6,7</sup>, Hyundeok Choi<sup>8,3</sup>, Andrew Tangborn<sup>8,3</sup>, Kai Wang<sup>9,3</sup>, Haixia Liu<sup>9,3</sup>, and Jeffrey Lee<sup>10</sup>

<sup>1</sup>Cooperative Institute for Research in Environmental Sciences, University of Colorado, Boulder, CO 80305, USA

<sup>2</sup>NOAA Global Systems Laboratory, Boulder, CO 80305, USA

<sup>3</sup>NOAA/NWS/NCEP/EMC, College Park, MD 20740, USA

<sup>4</sup>NASA Global Modeling and Assimilation Office, Greenbelt, MD 20771, USA

<sup>5</sup>Morgan State University, Baltimore, MD 21251, USA

<sup>6</sup>Center for Spatial Information Science and Systems, George Mason University, Fairfax, VA 22030, USA

<sup>7</sup>NOAA Air Resources Laboratory (ARL), College Park, MD 20740, USA

<sup>8</sup>SAIC@NOAA/NWS/NCEP/EMC, College Park, MD 20740, USA

<sup>9</sup>LINKER@NOAA/NWS/NCEP/EMC, College Park, MD 20740, USA

<sup>10</sup>School of Meteorology, University of Oklahoma, Norman, OK 73072, USA

**Correspondence:** Hongli Wang (hongli.wang@noaa.gov)

Received: 21 August 2025 – Discussion started: 29 September 2025

Revised: 22 February 2026 – Accepted: 11 March 2026 – Published: 27 March 2026

**Abstract.** This paper describes efforts to establish aerosol data assimilation capabilities for NOAA's National Air Quality Forecasting Capability (NAQFC), a regional online air quality modeling (AQM) system under NOAA's Unified Forecast System (UFS), by assimilating measurements of fine particulate matter (PM<sub>2.5</sub>, particles with aerodynamic diameters less than 2.5 μm). PM<sub>2.5</sub> assimilation is developed within the Joint Effort for Data assimilation Integration (JEDI) framework and tested using its 3D-Var data assimilation (DA) component. The PM<sub>2.5</sub> observation operator is constructed by combining newly developed PM<sub>2.5</sub> transformation recipes in the JEDI Variable Derivation Repository (VADER) with a general spatial interpolation operator in the Unified Forward Operator (UFO).

Cycled DA and forecast experiments were conducted from 1–21 September 2020, during a period of Western US wildfires, to assess the impact of assimilating PM<sub>2.5</sub> observations from the AirNow and PurpleAir networks. The control and analysis variables include individual aerosol species, with background error standard deviations generated by scaling their respective background values. Prognostic variables such as aerosol particle number and total particulate surface area

are updated accordingly following each analysis update. All DA experiments use a 3-hourly cycling interval, with PM<sub>2.5</sub> observations assimilated every 3 h. The control experiment uses the same configuration but without any data assimilation. Results show that assimilating either AirNow or PurpleAir PM<sub>2.5</sub> data reduces 1–24 h forecast errors in terms of mean absolute error (MAE) and root mean square error (RMSE) compared to the control run over Continental United States (CONUS). Substantial improvements are in regions where fire events took place and largely affected by transported smoke. Overall, the assimilation of PurpleAir observations in addition to AirNow data leads to a slight reduction in 3–24 h MAE.

## 1 Introduction

Particulate matter with an aerodynamic diameter of 2.5 μm or smaller (PM<sub>2.5</sub>) is a key contributor to poor air quality in the United States, posing significant risks to public health and the environment, and contributing to substantial loss of

life (Cohen et al., 2017; Colmer et al., 2020; Huang et al., 2025). Over the past few decades, poor air quality in the US has contributed to over 100 000 premature deaths annually, far exceeding fatalities from all other weather-related causes combined, which average around 500 per year (Huang et al., 2025). Given its public health significance, PM<sub>2.5</sub> is one of the important pollutants used in calculating the Air Quality Index (AQI) – a standardized system designed to communicate daily air pollution levels to the public at the US Environmental Protection Agency (EPA). Elevated PM<sub>2.5</sub> concentrations frequently result in “unhealthy” AQI ratings, triggering health advisories and public warnings.

PM<sub>2.5</sub> in the United States originates from a range of both anthropogenic and natural sources. Anthropogenic sources include agricultural activities and combustion processes, such as emissions from motor vehicles, power plants, industrial facilities, and residential heating systems. Among natural sources, wildfires are a particularly significant contributor, especially in the western United States, where their frequency and intensity have escalated dramatically over the past two decades (Wen and Burke, 2021). According to the US Environmental Protection Agency (EPA), wildfires account for approximately 15 % to 30 % of total PM<sub>2.5</sub> emissions nationwide (EPA, 2017). While national seasonal averages of PM<sub>2.5</sub> have generally declined, summer PM<sub>2.5</sub> concentrations in the western US have remained persistently high, primarily due to wildfire smoke (O'Dell et al., 2019). In addition to degrading air quality, wildfires have caused widespread property loss. Since 2005, more than 129 000 homes, businesses, and other structures have been destroyed by wildfire-related events (<https://headwaterseconomics.org/natural-hazards/structures-destroyed-by-wildfire>, last access: 18 February 2026), underscoring the urgent need for more effective strategies in air quality monitoring, forecasting, and wildfire management.

The National Oceanic and Atmospheric Administration (NOAA) has developed an advanced regional Air Quality Modeling (AQM) prediction system within the Unified Forecast System (UFS) framework to enhance the accuracy of air quality forecasts across the United States, particularly during wildfire events (Huang et al., 2025). The National Air Quality Forecast Capability (NAQFC), operated by NOAA's National Weather Service (NWS), has been providing operational air quality forecast guidance for over 20 years, with continuous inclusion of new capabilities. Under NAQFC, the AQM version 7 was implemented and became operational on 14 May 2024. The system features online coupling of atmospheric and chemical models, allowing dynamic interactions between meteorology and atmospheric chemistry. This integration improves the representation of emissions and ensures real-time feedback of meteorological fields that influence chemical transformations and the transport of pollutants in the atmosphere. The UFS-AQM online system has consistently shown improved performance in simulating major wildfire events, including the significant wildfires

in the northwestern coastal regions of the US in September 2020, and widespread smoke transport from Canadian wildfires in the summer of 2023. This system was officially implemented on 14 May 2024 as NOAA's operational air quality prediction system (AQMv7), replacing the previous offline-coupled Global Forecast System using the Finite Volume Cube-Sphere dynamical core (GFS-FV3) version 15 with the Community Multiscale Air Quality modeling system (CMAQv5.0.2) (Chen et al., 2021).

PM<sub>2.5</sub> data assimilation (DA) has proven effective in reducing errors in air quality forecasts (e.g., Pagowski et al., 2010, 2014; Schwartz et al., 2012; Wu et al., 2015; Robichaud, 2017; Sun et al., 2020; Lee et al., 2022; Chen et al., 2022; Ha, 2022; Park et al., 2022; Vogel et al., 2025, among others). Pagowski et al. (2010) demonstrated that fine aerosol forecasts benefit from AirNow PM<sub>2.5</sub> DA, showing improved verification scores for a period of at least 24 h. Schwartz et al. (2012) found that assimilating AirNow PM<sub>2.5</sub> observations significantly improved surface PM<sub>2.5</sub> forecasts over the CONUS compared to forecasts without DA. Wu et al. (2015) reported that incorporating ground-based PM<sub>2.5</sub> observations notably enhanced 24 h forecasts during a severe pollution episode in Shanghai. Similarly, Chen et al. (2022) showed that assimilating multi-source PM<sub>2.5</sub> data significantly improved WRF-Chem PM<sub>2.5</sub> forecasts with benefits lasting up to 48 h. Lee et al. (2021) highlighted the effectiveness of assimilating ground in-situ surface PM<sub>2.5</sub> observations in improving the short-term PM<sub>2.5</sub> predictions in Northeast Asia.

Many operational regional air quality prediction systems around the world use some form of data assimilation to initialize the forecasts. These approaches vary in complexity, ranging from simple optimal interpolation to full variational or ensemble Kalman filter methods (e.g. Robichaud et al., 2016; Wei et al., 2024; Colette et al., 2025). In NOAA's current regional air quality model (AQM) operations, aerosol and chemical initial conditions are “warm-started” using 6 h forecasts from the previous model cycle. The implementation of an aerosol data assimilation system can further enhance short-term air quality forecasts by providing more accurate spatial analyses of initial aerosol distributions.

To establish aerosol data assimilation capabilities for NOAA's regional operational AQM system, we employ the Joint Effort for Data assimilation Integration (JEDI) (Trémolet and Auligné, 2020). JEDI is a flexible, agnostic, and modern data assimilation system applicable to a wide range of forecasting systems (e.g. Liu et al., 2022; Huang et al., 2023; Sluka, 2024). JEDI offers a platform that supports efficient scientific development and facilitates the transition from research to operations. As part of a broader strategic shift, NOAA and partner agencies are transitioning their data assimilation systems to JEDI, opening the door for rapid integration of new scientific advancements, greater consistency across modeling systems, and enhanced collaboration across research communities and operational centers.

This study aims to develop and evaluate an initial aerosol analysis capability for the NOAA's regional AQM system by assimilating PM<sub>2.5</sub> observations using the JEDI three-dimensional variational (3D-Var) data assimilation framework. Compared to previous PM<sub>2.5</sub> data assimilation studies, this research adopts the NOAA's regional operational AQMv7 system and incorporates a new PM<sub>2.5</sub> transform in JEDI for assimilating PM<sub>2.5</sub> observations. In addition to evaluating the impact of assimilating AirNow PM<sub>2.5</sub> measurements on air quality prediction, this study also examines the impact of assimilating low-cost PurpleAir observations. Although PurpleAir data are valuable for PM<sub>2.5</sub> analysis (White et al., 2026) and real-time air quality monitoring, their potential impact on numerical air quality prediction remains insufficiently explored. To the authors' best knowledge, this is the first study to demonstrate the value of PurpleAir observations for air quality prediction during the wildfires of September 2020 using the AQMv7 system.

The paper is organized as follows: Sect. 2 provides a description of Methodology including the NOAA's AQM system, 3D-Var approach, and JEDI PM<sub>2.5</sub> assimilation. Experimental setup is presented in Sect. 3 including case description, AQM configuration, AirNow and PurpleAir PM<sub>2.5</sub> observations and background errors setup. Results are described in Sect. 4. A summary and discussion are presented in the final section.

## 2 Methodology

### 2.1 AQMv7 overview

The NOAA's regional operational AQMv7 system was developed through the online coupling of the Finite-Volume version 3 (FV3) dynamical core-based atmospheric model (Black et al., 2021) with the EPA's Community Multiscale Air Quality (CMAQ) model v5.2.0 within the UFS framework (Huang et al., 2025). In this UFS-AQM online system, CMAQ is treated as an atmospheric chemistry column model to simulate atmospheric chemistry reactions that govern concentrations of chemical species including gas- and aerosol-phase species. The transport terms of chemical species are handled by the FV3 dynamical core in the same way as other physics tracers (Huang et al., 2025). Aerosol module version 6 (AERO6) (Zhang et al., 2018) is utilized by CMAQ to simulate aerosol processes.

### 2.2 PM<sub>2.5</sub> assimilation within JEDI 3D-Var

In the JEDI framework, a series of components are provided to create a flexible, comprehensive data assimilation system (Trémolet and Auligné, 2020). The JEDI 3D-Var component is used to assimilate PM<sub>2.5</sub> for AQMv7. The 3D-Var method is chosen for its operational feasibility, primarily due to its low computational cost and the fact that it does not re-

quire an ensemble prediction system, as is needed in (hybrid) ensemble–variational data assimilation.

In practice, a 3D-Var data assimilation system typically uses an incremental approach to minimize a quadratic cost function which is defined in terms of the analysis increment  $\delta x$  relative to the guess state  $x_g$ :

$$J(\delta x) = \frac{1}{2}(\delta x - \delta x_g)\mathbf{B}^{-1}(\delta x - \delta x_g)^T + \frac{1}{2}(\mathbf{H}[\delta x] - \mathbf{d})\mathbf{R}^{-1}(\mathbf{H}[\delta x] - \mathbf{d})^T \quad (1)$$

Where:

- $\delta x_g = x_b - x_g$  is the guess state departure from background state, which is usually taken from a previous short-term forecast.
- $\mathbf{H}$  is the linearized observation operator of nonlinear observation operator  $H$ .
- $\mathbf{B}$  and  $\mathbf{R}$  are the background and observation error covariance matrices, respectively.
- $\mathbf{d}$  is the innovation vector, defined as:

$$\mathbf{d} = \mathbf{y} - H(x_g) \quad (2)$$

with  $\mathbf{y}$  representing the observation vector.

Once the increment  $\delta x$  is obtained, the analysis state  $x_a$  is reconstructed as:

$$x_a = x_g + \delta x \quad (3)$$

#### 2.2.1 PM<sub>2.5</sub> observation operator

To assimilate PM<sub>2.5</sub> data, a PM<sub>2.5</sub> transform that builds relationships between the model aerosol variables and the observed PM<sub>2.5</sub> needs to be developed. In AQMv7, the modal approach taken in the CMAQ model represents aerosol particle size distributions as the superposition of three lognormal modes: Aitken (I), accumulation (J), and coarse (K). It predicts only three integral properties of the size distribution for each mode: the total particle number concentration, the total surface area concentration, and the total mass concentration of the individual chemical components.

The total PM<sub>2.5</sub> concentration is calculated as a weighted sum of the individual aerosol concentration across these three modes:

$$\text{PM}_{2.5} = \text{ATOTI} \cdot \text{PM}_{25\text{AT}} + \text{ATOTJ} \cdot \text{PM}_{25\text{AC}} + \text{ATOTK} \cdot \text{PM}_{25\text{CO}} \quad (4)$$

Here, ATOTI, ATOTJ, and ATOTK represent the total aerosol mass concentrations in the Aitken, accumulation, and coarse modes, respectively. For example, ATOTI is the combined mass of 14 prognostic aerosol variables in the Aitken mode from the AERO6 aerosol module. Similarly, ATOTJ and ATOTK are the aggregated mass concentrations of 49 and 7

aerosol variables in the accumulation and coarse modes, respectively. PM<sub>25AT</sub>, PM<sub>25AC</sub>, and PM<sub>25CO</sub> are mass scaling factors for the three modes that vary by location and time. The aerosol variables within the same mode share the same mass scaling factor.

The PM<sub>2.5</sub> observation operator is constructed by combining the newly developed PM<sub>2.5</sub> transformation recipes in the JEDI Variable Derivation Repository (VADER) with an existing general spatial interpolation operator in the Unified Forward Operator (UFO). VADER is responsible for transforming model variables using user-defined “recipes” to generate new variables in model space. For PM<sub>2.5</sub> assimilation, VADER computes PM<sub>2.5</sub> from individual aerosol species using model-specific transformation, specifically using the Eq. (4) for this application. Since PM<sub>2.5</sub> composition varies by model, these transforms are implemented within VADER to match the specific structure of the regional air quality model AQMv7. Once PM<sub>2.5</sub> is derived in model space, UFO applies a generic spatial interpolation operator to map the model-simulated values to the observation locations, enabling computation of the observed minus forecast values.

The inputs for the PM<sub>2.5</sub> transformation are mixing ratio of the 70 aerosol variables with respect to dry air, the three mass scaling factors in the three modes, and dry air density for unit conversion. The output is the PM<sub>2.5</sub> in unit  $\mu\text{g m}^{-3}$ . It is noted that a new routine (recipe) has been added to VADER to derive dry air density from air temperature, pressure, and the specific gas constant for the dry air using the ideal gas law. This is applied in cases where the dry air density is not otherwise provided for the PM<sub>2.5</sub> calculation.

The new JEDI/VADER PM<sub>2.5</sub> recipe provides nonlinear (NL), tangent linear (TL), and adjoint (AD) transforms of PM<sub>2.5</sub> that keeps the output products in the same grid space as the input variables. Hence, the generic interpolation operator in UFO is used to connect the model-derived PM<sub>2.5</sub> fields with observed surface PM<sub>2.5</sub> measurements. This respects the JEDI paradigm of keeping the UFO component of the JEDI model independent.

### 2.2.2 Background error covariance modeling

In a 3D-Var system, the background error covariance (BEC) determines both the spatial spreading of information from observations, and the magnitude of the analysis increments along with the observation error variance.

The background error covariance matrix **B** can be decomposed into a standard deviation matrix (**Σ**) and a correlation matrix (**C**), as follows:

$$\mathbf{B} = \mathbf{\Sigma C \Sigma} \quad (5)$$

The correlation matrix **C** is generally non-diagonal. **Σ** is a diagonal matrix, with the standard deviations of the background errors for each variable on the diagonal.

The error modeling of the correlation matrix and standard deviations usually apply to control variables. In the

first implementation of aerosol data assimilation in JEDI for AQMv7, the control variables are defined as individual forecast aerosol variables, resulting in 70 control variables for AQMv7 with the AERO6 aerosol mechanism. The setup of background error standard deviation and correlation modeling will be described in Sect. 3: Experimental setup.

### 2.2.3 Minimization Algorithm (DRIPCG)

JEDI provides several minimization algorithm options. In this paper, we use the Derber–Rosati Inexact Preconditioned Conjugate Gradient (DRIPCG) algorithm (Derber and Rosati, 1989), as implemented in the JEDI's OOPS (Object-Oriented Prediction System) framework. DRIPCG has been extensively tested and is chosen here for stability and convergence efficiency.

## 3 Experimental setup

### 3.1 The September 2020 fire event and AQMv7 system setup

The wildfires of September 2020 ranked among the most intense in the US in recent years. These fires produced dense smoke that initially moved westward over the Willamette Valley in western Oregon and eventually blanketed the broader region. As a result, air quality rapidly across Oregon, Washington, and Idaho deteriorated to hazardous levels, marking one of the worst air quality periods in recent decades (Mass et al., 2022). Wildfire smoke originating from California, Oregon, and Washington was injected into the free troposphere and transported across the country by prevailing winds, leading to hazy conditions in several states. According to Li et al. (2021), from August to October 2020, wildfires in the western US contributed 23 % of surface PM<sub>2.5</sub> across CONUS, with higher contributions observed along the Pacific Coast (43 %) and in mountain region (42 %). This study focuses on the peak fire activity occurring between 1 and 21 September.

In this research, the model configuration is almost the same as the operational AQMv7 setup except for running over the CONUS domain with a 3-hourly cycling interval. The AQMv7 system is configured over the CONUS domain with a grid-spacing of 13 km and 65 vertical levels, extending up to 0.2 hPa. The system uses the Global Forecast System version 16 (GFSv16) physics package within the Common Community Physics Package (CCPP) framework to generate the meteorological fields driving air quality predictions. Meteorological initial conditions and lateral boundary conditions are generated using GFS forecast outputs with lead times up to 30 h at 3 h intervals from the previous GFS cycle. Fire-related emissions are represented using real-time Regional hourly Advanced Baseline Imager (ABI) and Visible Infrared Imaging Radiometer Suite (VIIRS) Emissions (RAVE) data at 0.03° spatial resolution. An-

thropogenic emissions are based on the 2016 US EPA NEI Collaborative (NEIC2016v1) modeling platform. Gas-phase chemistry is simulated using the Carbon Bond Mechanism version 6 (CB6r3) with updated isoprene chemistry and revised photolysis rates. More detailed information including physics, chemistry options, anthropogenic emissions, and fire emissions about the model configuration can be found in Huang et al. (2025).

### 3.2 PM<sub>2.5</sub> observations

In this study, surface PM<sub>2.5</sub> observations were obtained from two sources: AirNow and PurpleAir observing networks. These datasets differ in sensor type, spatial coverage, and quality control (QC) requirements. AirNow provides regulatory-grade measurements from federal, state, and local monitoring stations, while PurpleAir is a low-cost, community-based network of air quality sensors. PurpleAir sensors are widely deployed by individuals and communities, providing real-time data on PM<sub>2.5</sub> concentrations as well as meteorological variables such as temperature, pressure, and relative humidity. Only the data reported from outdoor PM<sub>2.5</sub> sensors are used in this study. The PurpleAir data were available for registered users through the PurpleAir API (<https://community.purpleair.com/t/api-use-guidelines/1589>, last access: 18 February 2026).

#### 3.2.1 PurpleAir PM<sub>2.5</sub> quality control

Quality control and correction of PurpleAir data followed the methodology described in Barkjohn et al. (2021). Readers are referred to that paper for further details. The following quality control (QC) filters were applied to the raw PurpleAir PM<sub>2.5</sub> measurements:

- Reported PM<sub>2.5</sub> values from two Plantower sensors within the PurpleAir sensor (channels A and B) must be nonnegative.
- The PurpleAir sensor channel A and B consistency:
  - Absolute difference  $< 5 \mu\text{g m}^{-3}$ , or
  - Relative difference within 61 %.
- PM<sub>2.5</sub> values must not exceed PM<sub>10</sub> values.
- PM<sub>2.5</sub> values must be less than  $3000 \mu\text{g m}^{-3}$  (upper threshold).
- Gross check of relative humidity with range 0 %–100 %.

Only PurpleAir PM<sub>2.5</sub> measurements that passed all the above QC criteria were retained for subsequent correction.

#### 3.2.2 PurpleAir PM<sub>2.5</sub> correction

A correction is required because the PurpleAir raw data usually overestimate PM<sub>2.5</sub> concentrations under typical ambient and smoke-impacted conditions. Correction of PurpleAir

PM<sub>2.5</sub> measurements was performed using a multiple linear regression model based on sensor-reported PM<sub>2.5</sub> (PA) and relative humidity (RH), following the correction formula proposed by Barkjohn et al. (2021):

$$\text{PM}_{2.5} = 0.524 \times \text{PA} - 0.0862 \times \text{RH} + 5.75 \quad (6)$$

We adopt the above equation because it was United States-wide valid by fitting data from September 2017 until January 2020. In addition, although the correction was originally derived for 24 h averaged PM<sub>2.5</sub>, it is consistent with a regression equation obtained from the September 2020 dataset based on 1 h averaged PM<sub>2.5</sub>.

#### 3.2.3 Observation error assignment

Observation error standard deviations were assigned to each network. The AirNow PM<sub>2.5</sub> observation errors were set to 5 % of the observed values. For PurpleAir PM<sub>2.5</sub> data, the observation errors were set to 10 % of the observed values to reflect the greater uncertainty typically associated with lower-cost sensors compared with regulatory AirNow monitors. The 10 % value is also consistent with the EPA definition of acceptable measurement uncertainty, which specifies a 10 % coefficient of variation for total precision (EPA, 2006).

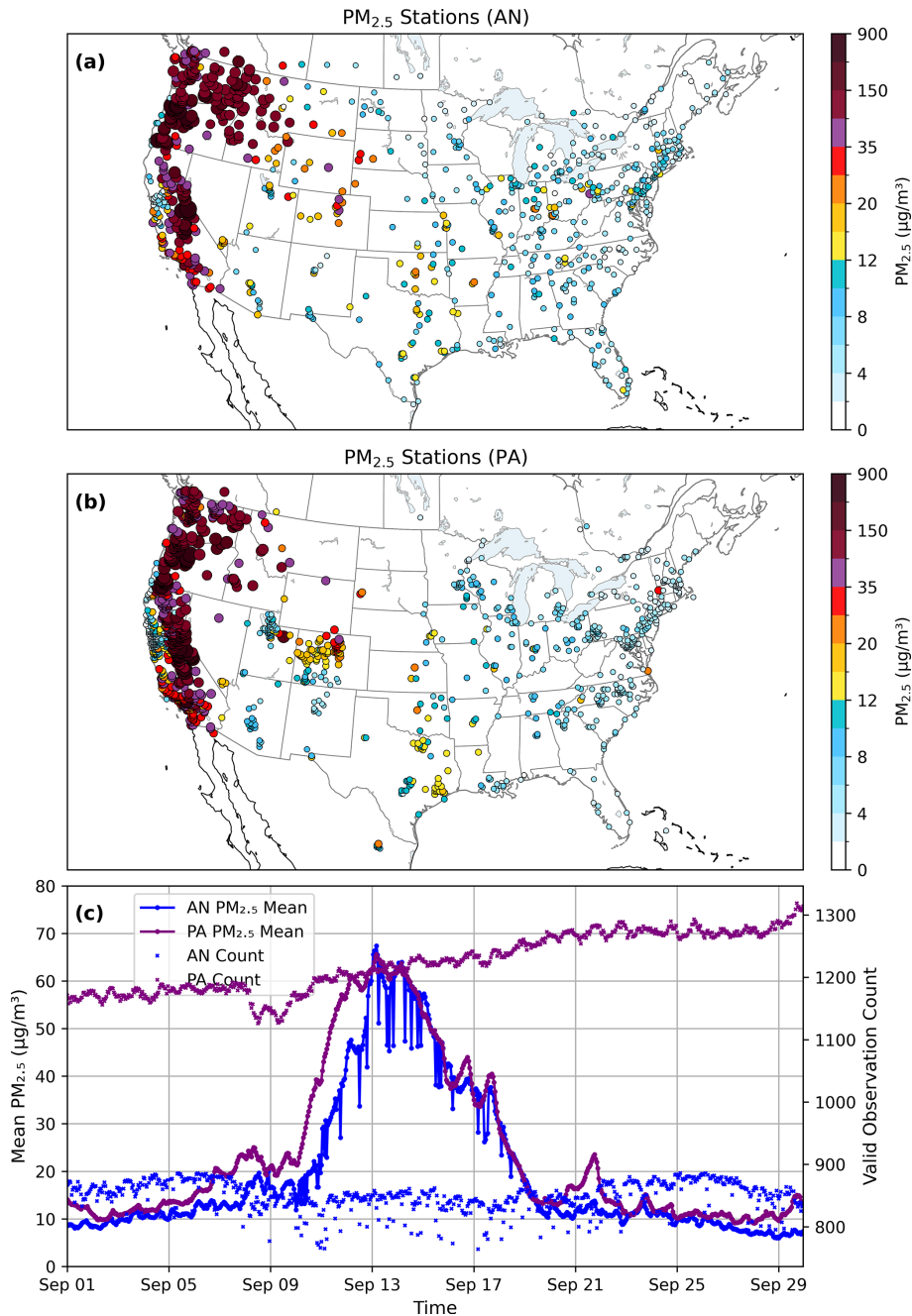
#### 3.2.4 Observation spatial distribution

Figure 1a and b shows the spatial distribution of AirNow and PurpleAir PM<sub>2.5</sub> monitoring stations at 12:00 UTC on 16 September 2020. PurpleAir sensors are especially concentrated in densely populated areas, leading to notable spatial variability in observation coverage during the September 2020 wildfire events. Coverage is particularly dense in urban regions of the western United States (e.g. California, Oregon, Washington, Utah, Arizona and Colorado), while rural and remote areas have significantly fewer sensors, for example, Nevada and North Dakota. Figure 1c displays the time series of domain averaged PM<sub>2.5</sub> values and station counts from the AirNow and PurpleAir networks. The number of AirNow stations ranges from approximately 800 to 900, while PurpleAir stations number between 1160 and 1300. Dropouts in the AirNow network lead to sudden decreases in station count and corresponding drops in the PM<sub>2.5</sub> time series. In contrast, the PurpleAir network shows a general upward trend in station count, with no major data dropouts observed.

### 3.3 Background error covariance

In this study, the background error standard deviation ( $\Sigma$ ) for each control variable is constructed based on the background forecast; specifically, the error standard deviations of an aerosol variable are prescribed as proportional to its background values.

The proportional scaling factor  $s$  is approximately estimated by building a linear relationship between the PM<sub>2.5</sub>



**Figure 1.** (a, b) Spatial distribution of AirNow(AN) and PurpleAir(PA) PM<sub>2.5</sub> monitoring stations on 12:00 UTC 16 September 2020. For PurpleAir, only stations that passed the quality control are shown. The displayed values are the corrected concentrations calculated using Eq. (6). (c) Time series of domain averaged PM<sub>2.5</sub> values and numbers from AirNow and PurpleAir observing networks.

standard error ( $\Sigma$ ) and the background forecast PM<sub>2.5</sub><sup>bkg</sup> concentrations:

$$\Sigma = s \cdot \text{PM}_{2.5}^{\text{bkg}} \quad (7)$$

The scaling factor  $s$  is subsequently applied to all PM<sub>2.5</sub> components, i.e., the 70 prognostic aerosol variables, to construct their error standard deviations.

This proportionality-based approach has also been adopted in the MOCAGE operational system (Colette et al., 2024), where background error standard deviations are similarly prescribed relative to background concentrations as a first-order approximation.

Tang et al. (2023) tested a similar method, in which the background PM<sub>2.5</sub> error variance is first estimated using the Hollingsworth–Lönnberg method (Hollingsworth and

Lönnerberg, 1986). A linear relationship is then established between the estimated PM<sub>2.5</sub> standard error and the background forecast PM<sub>2.5</sub><sup>bkg</sup>.

Here we take the same idea but using an alternative approach to roughly estimate the background PM<sub>2.5</sub> forecast error variance. The background PM<sub>2.5</sub> error variance ( $\Sigma^2$ ) is estimated using PM<sub>2.5</sub> innovation information  $\mathbf{d}$  defined in the Sect. 2.2, and observation error information  $\mathbf{R}$  specified in the Sect. 3.2.3, specifically,

$$\Sigma^2 = E(\mathbf{d}\mathbf{d}^T) - \mathbf{R} \quad (8)$$

In Eq. (8),  $E(\cdot)$  denotes the mathematical expectation operator. The superscript T denotes the transpose of a vector. Equation (8) is valid under the assumption that observation and background errors are uncorrelated. This assumption is reasonable when the innovation vector  $\mathbf{d}$  is calculated using forecasts from a free-running model without any aerosol data assimilation.

In this study, short-term (e.g., 3 h) PM<sub>2.5</sub> forecasts from a free run conducted during 1–21 September 2020 were used to compute the innovation vector  $\mathbf{d}$ . This free run, referred to as the *control run*, is described in detail in the following section. Using the innovations and observation errors from Sects. 2.2 and 3.2.3 as inputs to Eq. (8), the background error variance of PM<sub>2.5</sub> was first estimated. This error, along with the background values, was then used in Eq. (7) to estimate the scaling factor,  $s$ . This scaling factor was subsequently applied in all assimilation experiments presented in this study.

This proportionality-based approach implicitly assumes that displacement errors and severe background underprediction errors do not dominate, thereby focusing the assimilation process on correcting amplitude. It offers several benefits:

- It helps constrain analysis increments to physically meaningful regions. For example, it prevents the generation of sea salt aerosol increments over inland areas where no sea salt is present in the background. This is a problem that can occur when using GSI's height-dependent or latitude–height-dependent background error variance formulations, particularly when individual aerosol species are used as control variables.
- It introduces location- and time-dependent background error variance information, improving the realism of background error specification. Moreover, the aerosol variables that dominate background errors vary by location and assimilation cycle, rather than being consistently dominated by the same species when using constant static background error statistics. For example, organic and black carbon typically exhibit the largest errors in wildfire regions and downwind areas affected by smoke, whereas other regions may be dominated by non-organic aerosols.

An example of domain averaged background PM<sub>2.5</sub> error standard deviation from a data assimilation run that assimilated both AirNow and PurpleAir PM<sub>2.5</sub> is shown in Fig. 2.

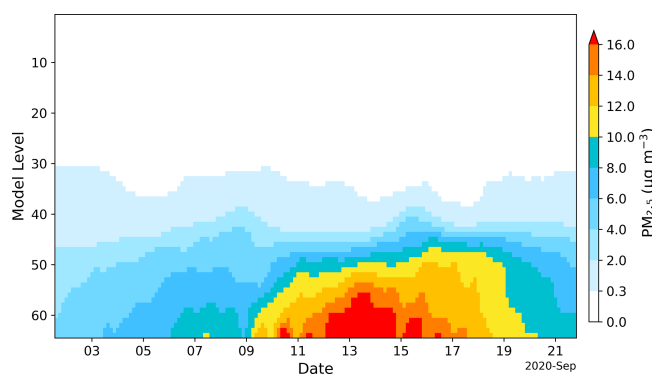


**Figure 2.** Domain averaged PM<sub>2.5</sub> error standard deviations for the data assimilation run that assimilated both AirNow and PurpleAir PM<sub>2.5</sub>.

lated both AirNow and PurpleAir PM<sub>2.5</sub> is shown in Fig. 2. This figure is intended to illustrate the main difference to static constant background errors, though the actual errors used in the data assimilation experiments are the errors of the individual aerosol control variables. It is obvious that this approach produces dynamically location- and time-dependent varying error estimates that yield particularly large error variances during the peak fire events from 10–20 September 2020.

The background error correlation matrix  $\mathbf{C}$  is modeled using a generic diffusion correlation operator designed for short length scales, as implemented in the System-Agnostic Background Error Representation (SABER) repository (Sluka, 2024). The primary input parameters are the horizontal and vertical cutoff length scales, defined as the distances beyond which correlations are zero. A horizontal cutoff scale of 100 km is applied, consistent with estimates derived from NMC statistics in previous GSI applications (Wang et al., 2021). For vertical correlations, this study uses a cutoff length scale of 12 model levels, which helps confine the influence of surface PM<sub>2.5</sub> observations within the average daytime planetary boundary layer (PBL) height ( $\sim 1450$  m) and has demonstrated improved surface PM<sub>2.5</sub> prediction as will be discussed in Sect. 4.

### 3.4 Update of total particle number and surface area concentrations

After the aerosol mass concentration has been analyzed, total particle number concentration and total surface area concentration can be updated accordingly. For simplicity, it is assumed that the ratio of the particle number concentration to total particulate volume within each mode (I, J, K) remains the same as in the background. Total particulate volume is used instead of mass mixing ratio because it is proportional to the particle number concentration (see Eq. 3 in Binkowski and Roselle, 2003). A similar assumption was adopted by Li

et al. (2013) to update number concentrations for the WRF-Chem model.

The number of particles is updated using the following relation:

$$N_a = \frac{N_b}{V_b} \times V_a \quad (9)$$

Where:

- $N_a$  and  $N_b$  are the number of particles in the analysis and background, respectively, within each mode.
- $V_a$  and  $V_b$  the total particulate volumes in the analysis and background, respectively, within the same mode.

The total particulate volume ( $V_a$  or  $V_b$ ) within each mode is calculated by dividing the mass concentration of each aerosol variable by its corresponding density in that mode, and then summing the results. This updating approach implicitly assumes that changes in volume across the three modes are driven solely by variations in particle number, rather than shifts in the aerosol size distribution. The total particulate surface area within each mode is then updated using the same volume ratio, i.e.,  $\frac{V_a}{V_b}$  multiplied by the background surface area.

In preparatory work for this study, six-hourly cycling experiments (Wang et al., 2025a) have shown that updating these variables is crucial for improving AQMv7 performance. In contrast, previous work using GSI with earlier developmental versions of AQM did not update these variables, primarily because those model versions were less advanced than the current operational AQMv7. As a result, there was still significant room for improving prediction skills.

### 3.5 Experiments

In the operational AQMv7 configuration, aerosol initial conditions (IC) are warm-started from a previous forecast cycle. In contrast, in cycling data assimilation and forecasting experiments, the data assimilation system provides aerosol initial conditions for the subsequent forecast, while the short-term (3 h) forecast serves as the background for the next data assimilation cycle. A schematic of the data assimilation and forecasting cycles is shown in Fig. 3.

In the assimilation cycle, JEDI updates the aerosol analysis by combining PM<sub>2.5</sub> observations with the background information. The updated aerosol analysis, together with meteorological initial conditions, emissions, and other inputs, is then used to initialize the subsequent forecasts in the forecast cycle. Note that the meteorological initial conditions are not updated by JEDI but are generated from GFS forecast outputs of the previous GFS cycle.

Four experiments were conducted to evaluate the performance of JEDI/AQM PM<sub>2.5</sub> DA. Table 1 provides a description of the experiments. The first experiment is a control run (CTR), in which meteorological initial and boundary conditions are updated every 3 h, while chemical and aerosol fields

are carried over from the 3 h forecast of the previous cycle. The other three experiments incorporate data assimilation: DA\_AN, DA\_PA, and DA\_ANPA, which assimilate AirNow PM<sub>2.5</sub> only, PurpleAir PM<sub>2.5</sub> only, and both AirNow and PurpleAir PM<sub>2.5</sub> observations, respectively.

Like the CTR experiment, all DA experiments are conducted as 3-hourly cycling runs. Data assimilation is performed every 3 h, and a 3 h forecast is launched at each cycle. This 3 h forecast serves as the background for the subsequent data assimilation and forecasting cycle. In addition, forecasts initialized at 00:00, 06:00, 12:00, and 18:00 UTC are extended to 24 h for evaluation purposes. The experimental period spans from 12:00 UTC on 1 September to 18:00 UTC on 21 September 2020. It is noted that to reduce random sensor noise and improve comparability with the model resolution ( $\sim 13$  km), the PurpleAir PM<sub>2.5</sub> data were spatially averaged onto a  $0.1^\circ \times 0.1^\circ$  latitude–longitude grid before assimilation.

## 4 Results

This section provides an overview of the impact of DA on PM<sub>2.5</sub> forecasts. A total of 80 forecasts – initialized four times daily from 00:00 UTC on 2 September to 18:00 UTC on 21 September 2020 – are used to evaluate model performance. AirNow PM<sub>2.5</sub> observations are used to verify the forecast. Forecast errors are assessed using bias, mean absolute error (MAE), and root mean square error (RMSE). Forecast performance is evaluated using box plots, which illustrate the distribution, spread, and central tendency of forecast errors. Time series of PM<sub>2.5</sub> at various forecast hours are presented to examine the temporal evolution of forecast performance. Additionally, spatial distributions of PM<sub>2.5</sub> including observations, forecasts, forecast errors, and forecast differences are analyzed to evaluate the spatial impact of data assimilation on PM<sub>2.5</sub> predictions.

Figure 4 presents the bias, mean absolute error (MAE), and root mean square error (RMSE) for the 1–24 h forecast of domain-averaged PM<sub>2.5</sub>. Domain averages are computed over all states in the mainland United States. From the bias statistics (Fig. 4a), it is seen that the bias in the control run follows an upward trend initially, then reverses into a downward trend. The data assimilation runs show a similar trend, as data assimilation primarily corrects the model state and does not fully resolve inherent model bias. The control run underpredicted surface PM<sub>2.5</sub> throughout the 24 h forecast period by about  $1 \mu\text{g m}^{-3}$ . This underprediction was improved in the data assimilation experiments. The two assimilated experiments, DA\_AN and DA\_ANPA, reduced the 1–24 h mean bias to  $-0.2$  and  $-0.3 \mu\text{g m}^{-3}$ , respectively. The PurpleAir PM<sub>2.5</sub> assimilation experiment (DA\_PA) also slightly improved the 1–24 h mean bias.

It is seen that DA\_PA produces a near zero bias at 1 h forecast, however this is due to large positive and negative biases canceling out. Therefore, it should be used together

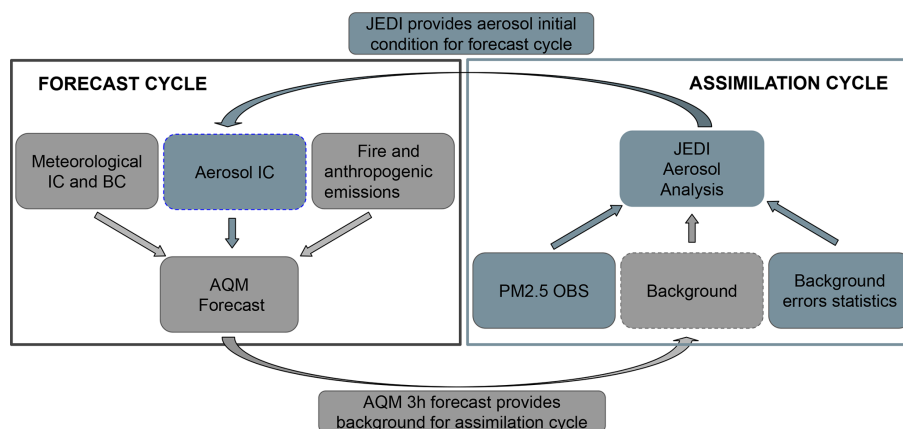


**Figure 3.** A schematic of the data assimilation and forecasting cycles.

**Table 1.** Descriptions of the experiments.

Experiment	Data Assimilation	PM <sub>2.5</sub> Observations Assimilated	Aerosol Fields
CTR	No	None	Carried over from previous cycle's 3 h forecast
DA_AN	Yes	AirNow PM <sub>2.5</sub> only	Updated by Assimilation
DA_PA	Yes	PurpleAir PM <sub>2.5</sub> only	Updated by Assimilation
DA_ANPA	Yes	AirNow + PurpleAir PM <sub>2.5</sub>	Updated by Assimilation

with norms like Mean Absolute Error (MAE) and Root Mean Square Error (RMSE), which quantify the actual magnitude of forecast errors.

In terms of MAE and RMSE, all the three data assimilation experiments reduced the surface PM<sub>2.5</sub> forecast error throughout the 24 h forecast period. The added value of assimilating PurpleAir PM<sub>2.5</sub> data alongside AirNow observations is evident in the consistent MAE reduction (Fig. 4b). Its impact on RMSE (Fig. 4c) is also positive, though relatively small. Overall, all the data assimilation experiments show improved forecast skill compared to the control run.

Figure 5 shows box-and-whisker plots of PM<sub>2.5</sub> forecast bias. Across all forecast hours, the interquartile range (IQR) – represented by the height of the boxes – is consistently smaller for the DA experiments compared to the control run. This indicates reduced forecast error spread between the 25th and 75th percentiles and suggests more consistent forecasts in the DA experiments. Although the median forecast bias in the control run is sometimes closer to zero, the DA\_ANPA experiment performs comparably in terms of central tendency while showing clear improvements in reducing the mean forecast bias, as also reflected in Fig. 4a. Among the DA experiments, DA\_AN and DA\_ANPA show the most consistent improvement at 24 h lead times, with DA\_ANPA slightly outperforming others during the early forecast hours (e.g., hour 1 to 12). This suggests that assimilating PurpleAir observations in addition to AirNow helps

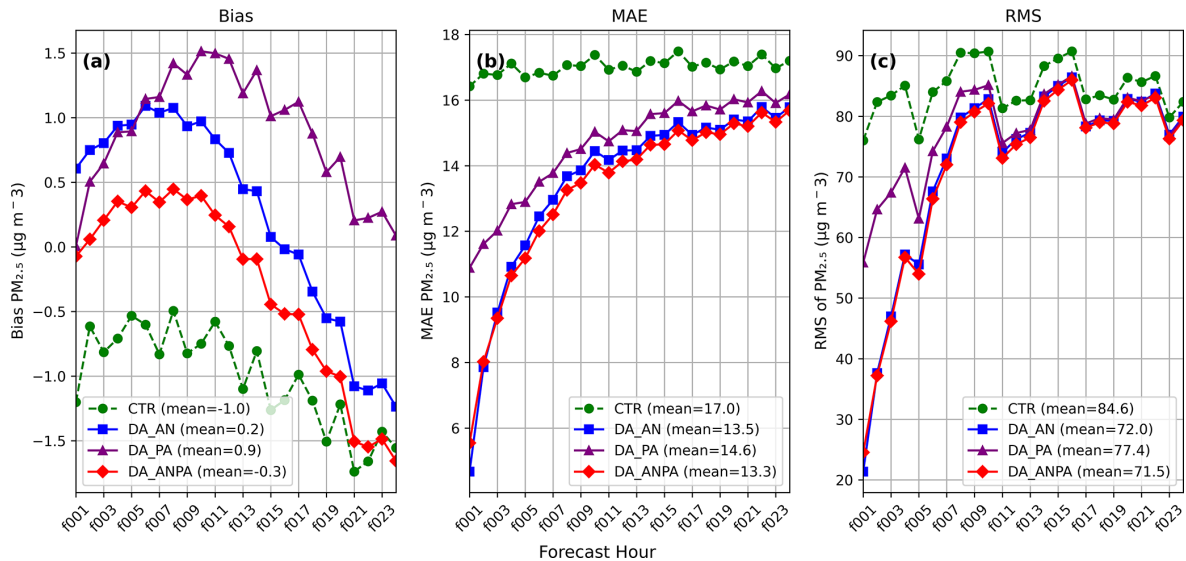
reduce bias and brings the forecasts closer to observed PM<sub>2.5</sub> values in the short term.

Figure 6 shows time series of PM<sub>2.5</sub> averaged over CONUS at forecast hours 1, 12, and 24, respectively. Consistent with the evaluations in Figs. 4 and 5, all DA experiments generally improve PM<sub>2.5</sub> forecasts. Notably, all DA experiments help correct underpredictions during 2–9 and 14–17 September. In addition, the substantial overprediction during 9–13 September observed in the control run is partially mitigated by the DA experiments. Among the DA experiments, DA\_AN and DA\_ANPA show comparable performance and both outperform DA\_PA.

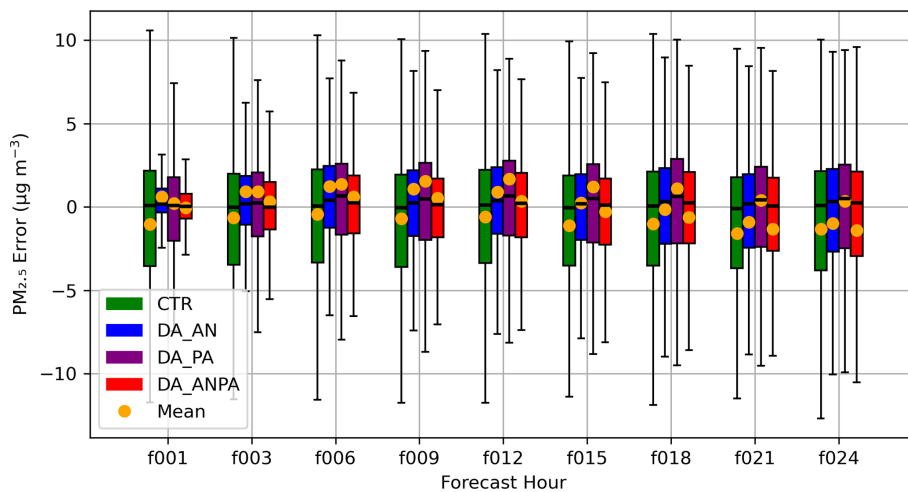
While we have investigated the impact of DA on PM<sub>2.5</sub> forecasts in terms of temporal evolution, it is also important to examine the spatial distribution of forecast fields, associated errors, and the impact of PM<sub>2.5</sub> data assimilation.

Figure 7 presents the spatial distribution of temporally averaged PM<sub>2.5</sub> forecasts at forecast hour 1, based on 80 forecasts initialized four times daily (00:00, 06:00, 12:00, and 18:00 UTC) from 2–21 September. The effects of wildfire events are clearly seen in Fig. 7a, c and e across California, Oregon, and Washington – where the fires occurred – as well as in downstream regions such as Montana, Wyoming, Utah, and Colorado impacted by smoke advection and transport.

1 h PM<sub>2.5</sub> forecast errors in the control run are evident in Fig. 6a but are more clearly highlighted in Fig. 7b, which shows the difference between the control run and AirNow observations. Significant overpredictions appear along the Cali-



**Figure 4.** PM<sub>2.5</sub> forecast errors for 1–24 h lead times based on 80 forecasts initialized four times daily during 2–21 September 2020. Domain-averaged over CONUS. The  $x$  axis represents forecast lead times from 1 to 24 h. **(a)** Bias, **(b)** Mean Absolute Error (MAE), **(c)** Root Mean Square Error (RMSE).



**Figure 5.** Box-and-whisker plot of PM<sub>2.5</sub> forecast bias. Orange dot: domain averaged mean; Bottom edge = Q1 (25th percentile); Top edge = Q3 (75th percentile); Height = Interquartile Range (IQR = Q3 – Q1); Horizontal line inside box: The median (50th percentile); Whiskers: Extend to the min and max values within  $1.5 \times$  IQR from Q1 and Q3.

fornia coast, as well as in parts of the Midwest and Northeast US, including Tennessee, Kentucky, West Virginia, and Virginia. Conversely, notable underpredictions are found over Colorado, New Mexico, much of Texas and Oklahoma, and several Gulf Coast states.

Both DA\_AN (Fig. 7c and d) and DA\_PA (Fig. 7e and f) show similar spatial correction patterns across California, Oregon, and Washington, particularly in reducing overpredictions along the California coast. They also produce comparable large-scale adjustments across the Northeast, Midwest, and Southern US, with their spatial patterns (Fig. 7d and f) largely opposite in sign to those in the CTR–AirNow

difference (Fig. 7b). This indicates that both DA experiments effectively mitigate the control run's over- and underpredictions.

However, the magnitude of the corrections is generally smaller in DA\_PA than in DA\_AN. DA\_PA shows its strongest impact over Nevada, northern Utah, Colorado, and southwestern New Mexico, where it helps alleviate regional underpredictions (Fig. 7e and f). These improvements are also observed in DA\_ANPA, whose spatial pattern closely resembles DA\_AN except over these few states (figures not shown).

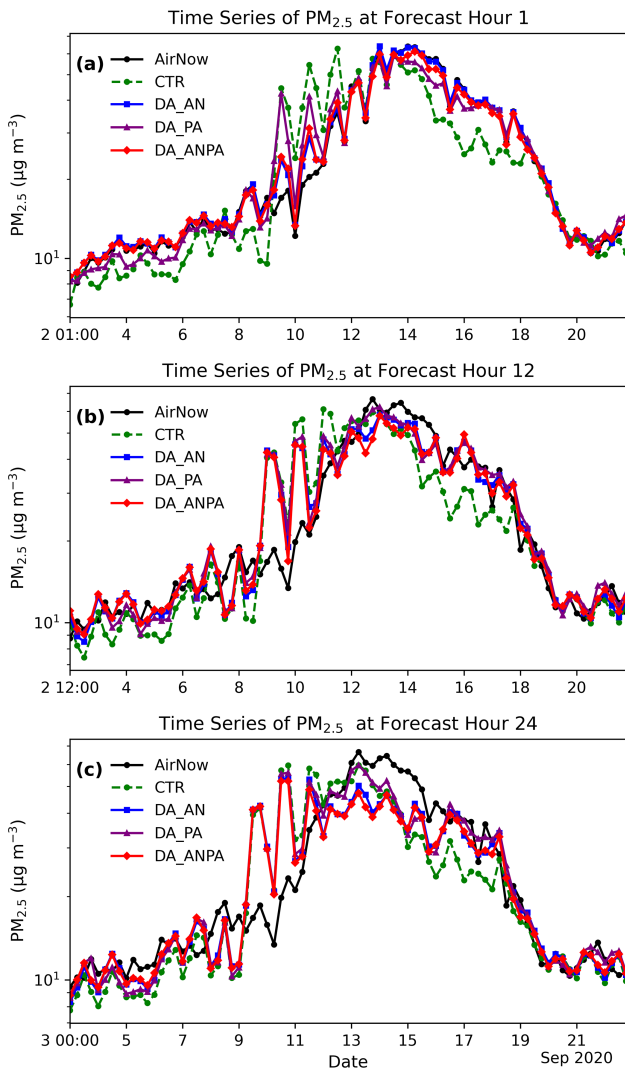


**Figure 6.** Time series of PM<sub>2.5</sub> averaged over CONUS for (a) forecast hour 1, (b) forecast hour 12, and (c) forecast hour 24. The y axis is shown on a logarithmic scale.

The above analysis shows that data assimilation effectively corrects the 1 h forecast errors in the control run, particularly in the DA\_AN and DA\_ANPA experiments. It is therefore of interest to examine how data assimilation affects longer forecast lead times. Figure 8 presents the MAE from the CTR experiment and the percentage change in MAE (%) between the data assimilation (DA) experiments and the CTR experiment at the 24 h forecast lead time. Negative values in Fig. 8b–d indicate a reduction in MAE.

It is seen from Fig. 8a that the largest MAE values occur in California, Oregon, Washington, Idaho, Montana, Wyoming, Utah, Colorado, and Arizona. The PM<sub>2.5</sub> MAE in these states is generally greater than 10 µg m<sup>-3</sup>, with maximum values exceeding 150 µg m<sup>-3</sup> at certain stations in California, Ore-

gon, and Washington. In contrast, regions less affected by wildfire smoke exhibit MAE values below 10 µg m<sup>-3</sup>.

All DA experiments (Fig. 8b–d) show overall reductions in MAE at most stations. MAE reduction varies by location, with substantial improvements observed in regions with large forecast errors, such as California, Oregon, Washington, and Idaho, where MAE is reduced by approximately 20%. On average, assimilation of AirNow PM<sub>2.5</sub> observations alone significantly improves the 24 h forecast skill, with MAE reductions of 6.6% based on MAE percentage changes averaged over all stations. In contrast, assimilation of PurpleAir data alone reduces the MAE by only 1.7%. Assimilating both AirNow and PurpleAir PM<sub>2.5</sub> observations reduces the MAE by 7.6%, indicating that PurpleAir data provides complementary value to AirNow in improving forecast skill.

In the DA\_PA experiment, a few eastern coastal states from Georgia to Virginia exhibit large percentage increases in MAE. These increases are associated with relatively small absolute errors, as MAE values in the CTR experiment over these states are typically only 2–4 µg m<sup>-3</sup> (Fig. 8a). Increased MAE is also present at several stations at the 1 h forecast lead time in the DA\_PA experiment in these areas (figure not shown). In contrast, the MAE increase at the 24 h forecast lead time is much less pronounced in the experiment assimilating only AirNow PM<sub>2.5</sub> observations. This behavior suggests potential quality issues in the assimilated PurpleAir data in those areas that require further investigation, although a contribution from model errors cannot be ruled out.

To further examine model performance across different regions, error statistics (bias, MAE, and RMSE) for the averaged 1–24 h PM<sub>2.5</sub> forecasts from the control and data assimilation experiments over the 10 EPA regions are analyzed. Figure 9 presents the EPA Regions 1–10 and Averaged 1–24 h PM<sub>2.5</sub> forecasts errors statistics in each EPA region.

In terms of bias (Fig. 9b), the DA\_AN and DA\_ANPA forecasts show improved performance relative to the control run. The DA\_PA experiment also improves bias over most EPA regions, except for increased overprediction in EPA regions 8 and 9. For MAE and RMSE, the DA\_AN and DA\_ANPA experiments generally show improved performance across all EPA regions. The DA\_PA experiment also exhibits improved, or at least comparable, MAE relative to the control run. However, DA\_PA shows slightly increased RMSE over EPA regions 1–4, while reduced RMSE is found over other EPA regions.

Substantial reductions in MAE and RMSE are observed over EPA regions 8–10, where fire events occurred and/or where regions were most influenced by transported smoke. This is consistent with the large 1 h MAE reduction shown in Fig. 8. Notably, the DA\_PA experiment, which assimilates PA observations alone, reduces both MAE and RMSE over EPA regions 8–10. Assimilating PurpleAir data together with AirNow data results in slightly smaller MAE and RMSE over these regions, suggesting that PurpleAir observations

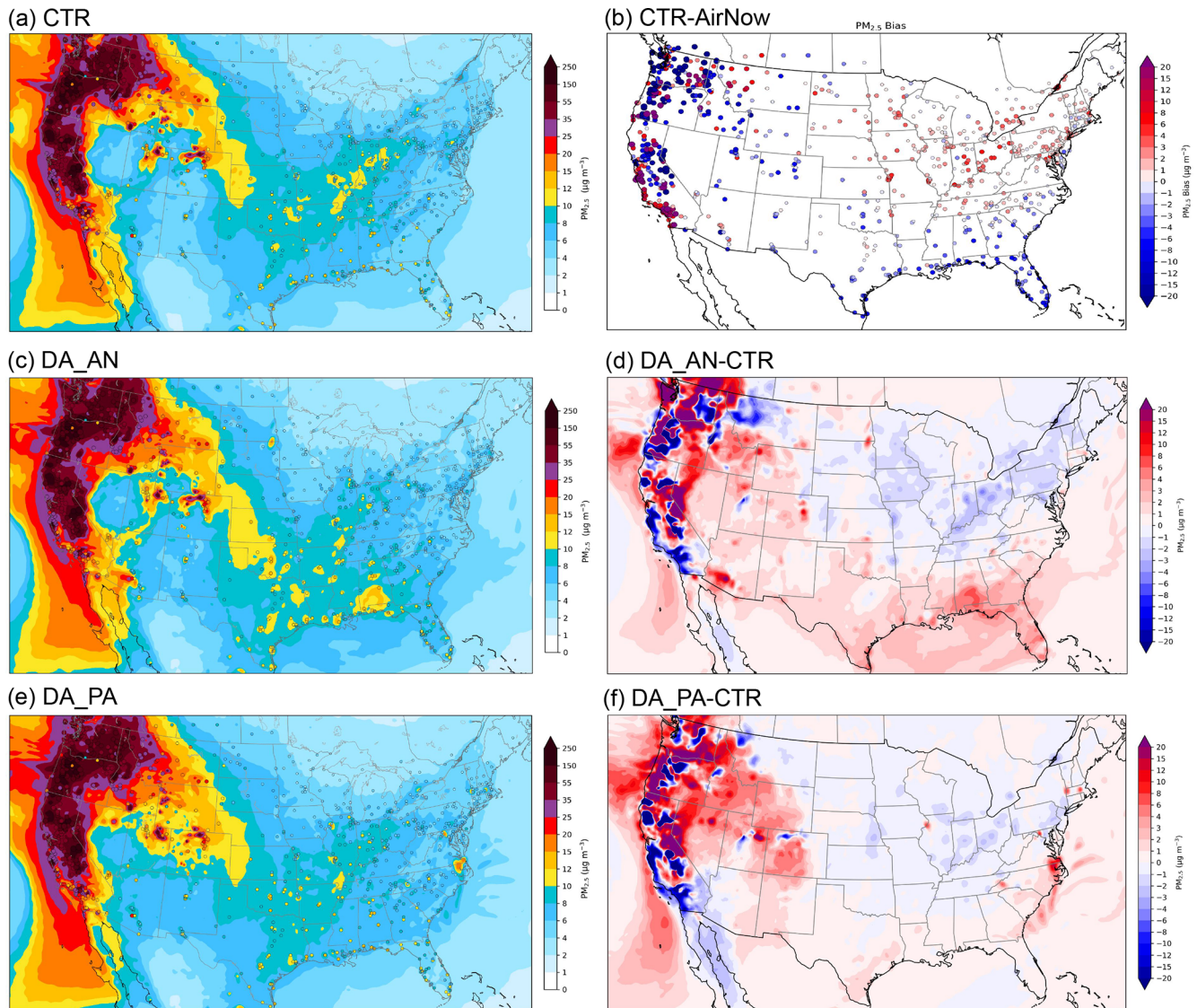


**Figure 7.** Spatial distribution of average PM<sub>2.5</sub> at forecast hour 1, based on 80 forecasts initialized four times daily (00:00, 06:00, 12:00, and 18:00 UTC) during 2–21 September. (a) PM<sub>2.5</sub> in experiment CTR (shaded) overlaid with AirNow PM<sub>2.5</sub> observations (filled dots). (b) PM<sub>2.5</sub> bias in experiment CTR. (c) PM<sub>2.5</sub> in experiment DA\_AN (shaded) overlaid with AirNow PM<sub>2.5</sub> observations. (d) PM<sub>2.5</sub> difference between experiments DA\_AN and CTR. (e) PM<sub>2.5</sub> in experiment DA\_PA (shaded) overlaid with AirNow PM<sub>2.5</sub> observations. (f) PM<sub>2.5</sub> difference between experiments DA\_PA and CTR.

nonetheless provide complementary information to AirNow in these regions.

## 5 Summary and discussion

The latest version of NOAA's regional AQM system became operational on 14 May 2024. This system is based on the online coupling of the FV3 atmospheric model with the CMAQ model within the UFS framework. To improve initial conditions for AQM and enhance predictions of wildfire impacts on air quality, the capability to assimilate PM<sub>2.5</sub> observations into AQMv7 was developed within JEDI and evaluated using

its 3D-Var assimilation component in this study. The developed assimilation scheme can also be used to generate analysis (reanalysis) dataset for other applications, for example, providing data for training artificial intelligent models used in air quality prediction.

Data assimilation experiments were conducted for the September 2020 Western US wildfire episode, using 3-hourly cycling with observations from the AirNow and PurpleAir networks. In the data assimilation experiments, the location- and time-dependent background error standard deviations of an aerosol variable are specified as proportional to its background values, using a diagnosed scaling factor. In addition

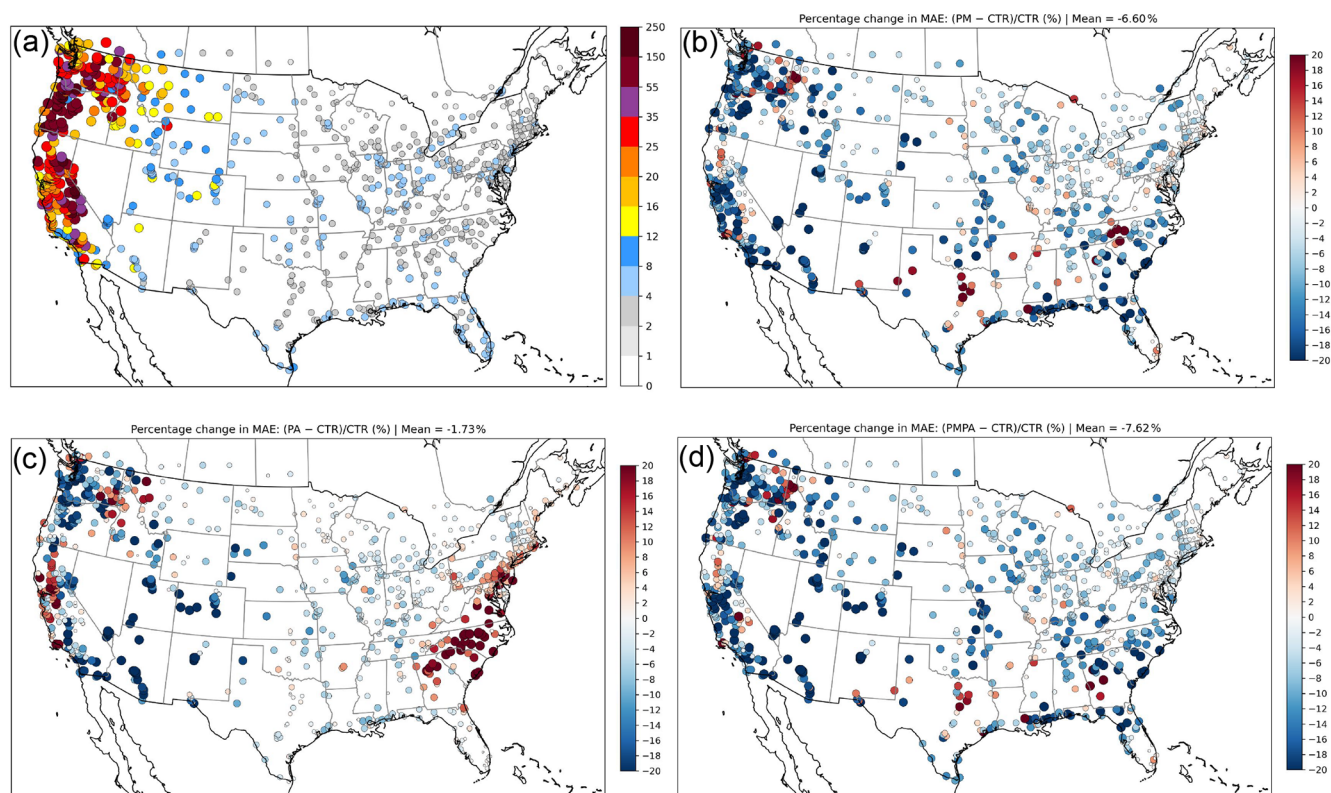


**Figure 8.** (a) MAE from the control (CTR) experiment. Percentage change in MAE (%) relative to CTR for (b) DA\_AN, (c) DA\_PA, and (d) DA\_ANPA. The percentage change is calculated as  $(MAE(DA) - MAE(CTR)) / MAE(CTR) \times 100$ .

to updating the analyzed aerosol variables in each mode, the particle number concentration and surface area of each mode are also updated. The results show that assimilating AirNow PM<sub>2.5</sub> observations improves 1–24 h forecast skill. Assimilating PurpleAir data alone yields modest improvements in MAE. Combining PurpleAir with AirNow observations provides additional benefit by slightly further reducing MAE relative to AirNow-only assimilation, indicating that PurpleAir observations nonetheless provide complementary information to AirNow. The AirNow data assimilation alone or with PurpleAir data generally show reduced MAE and RMSE across all EPA regions, whereas the largest reductions in MAE and RMSE are observed over regions affected by fire events and/or strongly influenced by transported smoke. The positive impact of PurpleAir data assimilation on smoke prediction during the September 2020 wildfires has also been demonstrated in an experimental Rapid Refresh Forecast System coupled with the Smoke and Dust Model (Wang et al., 2023), where it significantly reduced the model's 24 h underprediction of surface PM<sub>2.5</sub>. Given that PurpleAir data coverage has improved since September 2020, the results of this study further highlight its potential to complement AirNow observations by filling spatial gaps and improving PM<sub>2.5</sub> analysis and forecast skill.

In this initial development and evaluation of aerosol data assimilation in JEDI for AQMv7, the control variables are defined as individual forecast aerosol variables. In previous work on aerosol data assimilation for an earlier version of AQM using the GSI system (Wang et al., 2021), one option for the control variables was to define them as the total aerosol mass in each of the three modes, resulting in just three control variables. A control variable transform was then applied to partition the analysis increments across these modes to individual aerosol species, based on the ratio of each species' mass to the total mass within the corresponding mode. The use of total aerosol mass in the three modes as control variables – thereby reducing the number of control variables from 70 to 3 – is planned for a future phase of development. The use of total masses as control variables also reduces the cost of the background error statistics calculation and iterative minimization (Kumar et al., 2019).

This study focused on surface-level PM<sub>2.5</sub> and did not incorporate vertical profile constraints with satellite-based aerosol optical depth (AOD) retrievals, which could further enhance forecast skill. A key challenge is the need for a robust forward operator in the CRTM AOD module – specifically, the creation and validation of lookup tables (LUTs) for AOD calculations with AQM. As an intermediate solution, existing LUTs in CRTM, such as the GEOS-5 LUTs,

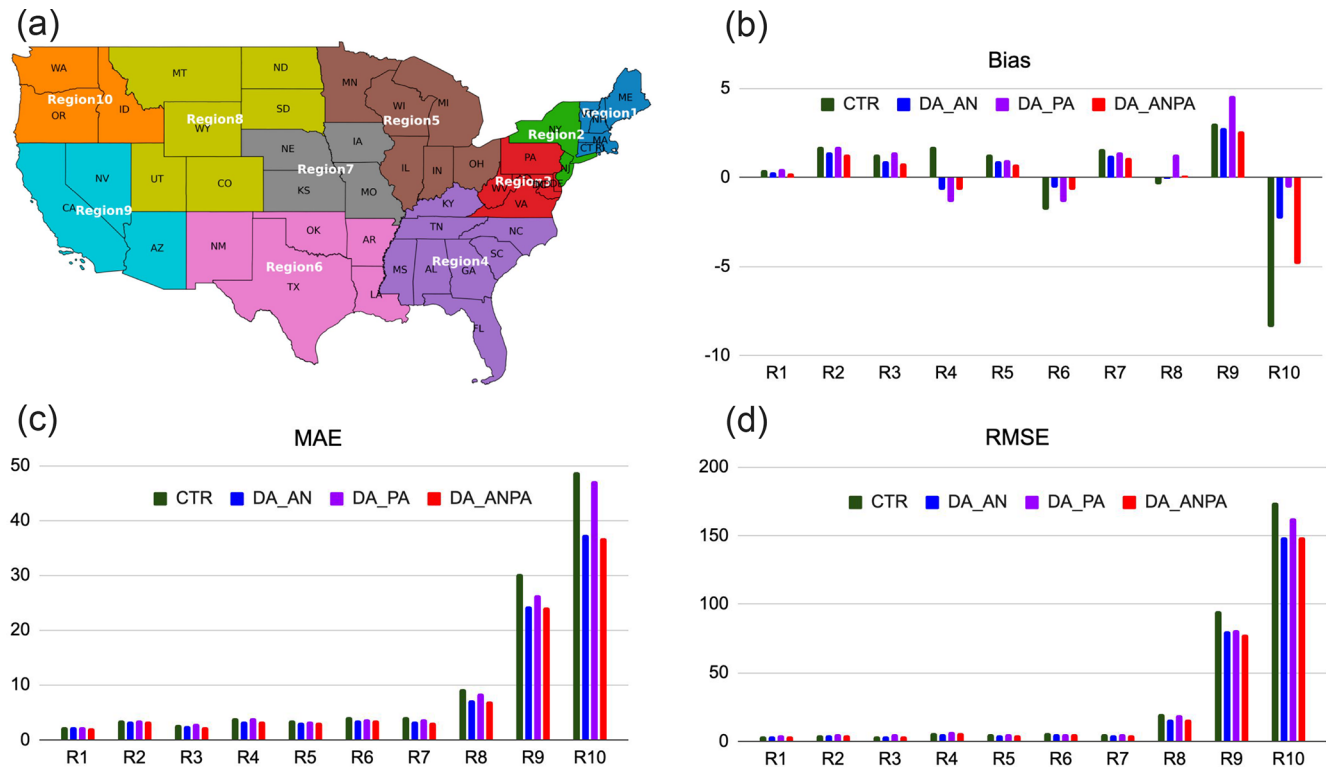


**Figure 9.** (a) EPA Regions 1–10. Averaged 1–24 h PM<sub>2.5</sub> forecasts errors: (b) Bias, (c) MAE and (d) RMSE.

have been tested by grouping and mapping AQM aerosol species to those used in GEOS-5 (Wang et al., 2025). AOD assimilation also depends on an accurate vertical distribution of aerosols in the background field so that the CRTM AOD operator can provide meaningful gradient information at the correct vertical levels to constrain the analysis update. However, AQM models have shown deficiencies for the September 2020 fire events in representing smoke concentrations at and above plume rise levels, largely due to how fire emissions are injected into the model. This will be improved in the next update of the operational AQM.

**Code and data availability.** The AQMV7 model, JEDI software and PM<sub>2.5</sub> and fire emission data we used in this research are publicly available on Zenodo (<https://doi.org/10.5281/zenodo.17049857>, Wang et al., 2025b).

Users are referred to the guidance on compiling and running the model: (<https://ufs-srweather-app.readthedocs.io/en/develop/UsersGuide/index.html>, last access: 26 August 2025). Global Forecast System analysis data were downloaded from the NCAR Research Data Archive: <https://doi.org/10.5065/D65D8PWK> (DOC/NOAA/NWS/NCEP, 2015).

**Author contributions.** HW designed and developed the PM<sub>2.5</sub> DA capability within JEDI for the AQM model, conducted experiments, and evaluated performance; CM and JB contributed to PM<sub>2.5</sub> DA

methodology, advised on code implementation, and assisted in performance analysis; SW contributed to PM<sub>2.5</sub> DA methodology and experimental design; RL conducted control experiments and contributed to workflow development; JL and KW contribute to model configuration and control run setup; YT contributed to background error modeling and observational error specification; HC, AT and HL contributed to workflow development; JL performed quality control and correction of PurpleAir observations.

**Competing interests.** The contact author has declared that none of the authors has any competing interests.

**Disclaimer.** The scientific results and conclusions, as well as any views or opinions expressed herein, are those of the authors and do not necessarily reflect those of NOAA or the Department of Commerce.

**Publisher's note:** Copernicus Publications remains neutral with regard to jurisdictional claims made in the text, published maps, institutional affiliations, or any other geographical representation in this paper. The authors bear the ultimate responsibility for providing appropriate place names. Views expressed in the text are those of the authors and do not necessarily reflect the views of the publisher.

**Acknowledgements.** The authors sincerely thank Dr. Ming Hu and the three anonymous reviewers for their constructive comments and insightful suggestions, which significantly improved the quality and clarity of this manuscript. The authors also thank Mohammed Farooqui at Texas A&M University-Kingsville for assisting with Python scripts to download the PurpleAir observations.

**Financial support.** This research was supported by the Fire Weather and Precipitation Research and Development in Support of the Disaster Relief Supplemental Appropriations Act (DRSA) project (NA23OAR4050200D), and in part by a NOAA Cooperative Agreement NA22OAR4320151 with the University of Colorado.

**Review statement.** This paper was edited by Narendra Ojha and reviewed by three anonymous referees.

## References

- Barkjohn, K. K., Gantt, B., and Clements, A. L.: Development and application of a United States-wide correction for PM<sub>2.5</sub> data collected with the PurpleAir sensor, *Atmos. Meas. Tech.*, 14, 4617–4637, <https://doi.org/10.5194/amt-14-4617-2021>, 2021.
- Binkowski, F. S. and Roselle, S. J.: Models-3 Community Multiscale Air Quality (CMAQ) model aerosol component, 1, Model description, *J. Geophys. Res.-Atmos.*, 108, 4183, <https://doi.org/10.1029/2001JD001409>, 2003.
- Black, T. L., Abeles, J. A., Blake, B. T., Jovic, D., Rogers, E., Zhang, X., Aligo, E. A., Dawson, L. C., Lin, Y., Strobach, E., Shafran, P. C., and Carley, J. R.: A limited area modeling capability for the finite-volume cubed-sphere (FV3) dynamical core and comparison with a global two-way nest, *J. Adv. Model. Earth Sy.*, 13, e2021MS002483, <https://doi.org/10.1029/2021MS002483>, 2021.
- Chen, L., Mao, F., Hong, J., Zang, L., Chen, J., Zhang, Y., Gan, Y., Gong, W., and Xu, H.: Improving PM<sub>2.5</sub> predictions during COVID-19 lockdown by assimilating multi-source observations and adjusting emissions, *Environ. Pollut.*, 297, 118783, <https://doi.org/10.1016/j.envpol.2021.118783>, 2022.
- Chen, X., Zhang, Y., Wang, K., Tong, D., Lee, P., Tang, Y., Huang, J., Campbell, P. C., McQueen, J., Pye, H. O. T., Murphy, B. N., and Kang, D.: Evaluation of the offline-coupled GFSv15–FV3–CMAQv5.0.2 in support of the next-generation National Air Quality Forecast Capability over the contiguous United States, *Geosci. Model Dev.*, 14, 3969–3993, <https://doi.org/10.5194/gmd-14-3969-2021>, 2021.
- Cohen, A. J., Brauer, M., Burnett, R., Anderson, H. R., Frostad, J., Estep, K., Balakrishnan, K., Brunekreef, B., Dandona, L., Dandona, R., Feigin, V., Freedman, G., Hubbell, B., Jobling, A., Kan, H., Knibbs, L., Liu, Y., Martin, R., Morawska, L., Pope, C. A., Shin, H., Straif, K., Shaddick, G., Thomas, M., van Dingenen, R., van Donkelaar, A., Vos, T., Murray, C. J. L., and Forouzanfar, M. H.: Estimates and 25 year trends of the global burden of disease attributable to ambient air pollution: an analysis of data from the Global Burden of Diseases Study 2015, *Lancet*, 389, 1907–1918, 2017.
- Colette, A., Collin, G., Besson, F., Blot, E., Guidard, V., Meleux, F., Royer, A., Petiot, V., Miller, C., Fermond, O., Jeant, A., Adani, M., Arteta, J., Benedictow, A., Bergström, R., Bowdalo, D., Brandt, J., Briganti, G., Carvalho, A. C., Christensen, J. H., Couvidat, F., D'Elia, I., D'Isidoro, M., Denier van der Gon, H., Descombes, G., Di Tomaso, E., Douros, J., Escribano, J., Eskes, H., Fagerli, H., Fatahi, Y., Flemming, J., Friese, E., Frohn, L., Gauss, M., Geels, C., Guarnieri, G., Guevara, M., Guion, A., Guth, J., Hänninen, R., Hansen, K., Im, U., Janssen, R., Jeoffrion, M., Joly, M., Jones, L., Jorba, O., Kadantsev, E., Kahnert, M., Kaminski, J. W., Kouznetsov, R., Kranenburg, R., Kuenen, J., Lange, A. C., Langner, J., Lannuque, V., Macchia, F., Manders, A., Mircea, M., Nyiri, A., Olid, M., Pérez García-Pando, C., Palamarchuk, Y., Piersanti, A., Raux, B., Razinger, M., Robertson, L., Segers, A., Schaap, M., Siljamo, P., Simpson, D., Sofiev, M., Stangel, A., Struzewska, J., Tena, C., Timmermans, R., Tsikerdekis, T., Tsyro, S., Tyuryakov, S., Ung, A., Uppstu, A., Valdebenito, A., van Velthoven, P., Vitali, L., Ye, Z., Peuch, V.-H., and Rouil, L.: Copernicus Atmosphere Monitoring Service – Regional Air Quality Production System v1.0, *Geosci. Model Dev.*, 18, 6835–6883, <https://doi.org/10.5194/gmd-18-6835-2025>, 2025.
- Colmer, J., Hardman, I., Shimshack, J., and Voorheis, J.: Disparities in PM<sub>2.5</sub> air pollution in the United States, *Science*, 369, 575–578, <https://doi.org/10.1126/science.aaz9353>, 2020.
- Derber, J. C. and Rosati, A.: A global ocean data assimilation system, *J. Phys. Oceanogr.*, 19, 1333–1347, [https://doi.org/10.1175/1520-0485\(1989\)019<1333:AGODAS>2.0.CO;2](https://doi.org/10.1175/1520-0485(1989)019<1333:AGODAS>2.0.CO;2), 1989.
- DOC/NOAA/NWS/NCEP: National Centers for Environmental Prediction, National Weather Service, NOAA, U.S. Department of Commerce, NCEP GFS 0.25 Degree Global Forecast Grids Historical Archive, NSF National Center for Atmospheric Research [data set], <https://doi.org/10.5065/D65D8PWK>, 2015.
- Environmental Protection Agency: Technical Note on Reporting PM<sub>2.5</sub> Continuous Monitoring and Speciation Data to the Air Quality System (AQS), <https://www.epa.gov/aqs/aqs-memos-technical-note-reporting-pm25-continuous-monitoring-and-speciation-data-air-quality> (last access: 24 March 2026), 8 November 2006.
- EPA: Wildfire and Air Quality, US Environmental Protection Agency, [https://www.epa.gov/sites/default/files/2018-08/documents/epa-2018-science\\_annualreport\\_508compressed.pdf](https://www.epa.gov/sites/default/files/2018-08/documents/epa-2018-science_annualreport_508compressed.pdf) (last access: 24 March 2026), 2017.
- Ha, S.: Implementation of aerosol data assimilation in WRFDA (v4.0.3) for WRF-Chem (v3.9.1) using the RACM/MADE-VBS scheme, *Geosci. Model Dev.*, 15, 1769–1788, <https://doi.org/10.5194/gmd-15-1769-2022>, 2022.
- Hollingsworth, A. and Lönnberg, P.: The statistical structure of short-range forecast errors as determined from radiosonde data, Part I: The wind field, *Tellus A*, 38, 111–136, <https://doi.org/10.1111/j.1600-0870.1986.tb00460.x>, 1986.
- Huang, B., Pagowski, M., Trahan, S., Martin, C. R., Tangborn, A., Kondragunta, S., and Kleist, D. T.: JEDI-based three-dimensional Ensemble-Variational Data Assimilation System for global aerosol forecasting at NCEP, *J. Adv. Model. Earth Sy.*, 15, e2022MS003232, <https://doi.org/10.1029/2022MS003232>, 2023.
- Huang, J., Stajner, I., Montuoro, R., Yang, F., Wang, K., Huang, H.-C., Jeon, C.-H., Curtis, B., McQueen, J., Liu, H.,

- Baker, B., Tong, D., Tang, Y., Campbell, P., Grell, G., Frost, G., Schwantes, R., Wang, S., Kondragunta, S., Li, F., and Jung, Y.: Development of the next-generation air quality prediction system in the unified forecast system framework: enhancing predictability of wildfire air quality impacts, *B. Am. Meteorol. Soc.*, <https://doi.org/10.1175/BAMS-D-23-0053.1>, 2025.
- Lee, S., Song, C. H., Han, K. M., Henze, D. K., Lee, K., Yu, J., Woo, J.-H., Jung, J., Choi, Y., Saide, P. E., and Carmichael, G. R.: Impacts of uncertainties in emissions on aerosol data assimilation and short-term PM<sub>2.5</sub> predictions over Northeast Asia, *Atmos. Environ.*, 271, 118921, <https://doi.org/10.1016/j.atmosenv.2021.118921>, 2022.
- Li, Y., Tong, D., Ma, S., Zhang, X., Kondragunta, S., Li, F., and Saylor, R.: Dominance of wildfires impact on air quality exceedances during the 2020 record-breaking wildfire season in the United States, *Geophys. Res. Lett.*, 48, e2021GL094908, <https://doi.org/10.1029/2021GL094908>, 2021.
- Li, Z., Zang, Z., Li, Q. B., Chao, Y., Chen, D., Ye, Z., Liu, Y., and Liou, K. N.: A three-dimensional variational data assimilation system for multiple aerosol species with WRF/Chem and an application to PM<sub>2.5</sub> prediction, *Atmos. Chem. Phys.*, 13, 4265–4278, <https://doi.org/10.5194/acp-13-4265-2013>, 2013.
- Liu, Z., Snyder, C., Guerrette, J. J., Jung, B.-J., Ban, J., Vahl, S., Wu, Y., Trémolet, Y., Auligné, T., Ménétrier, B., Shlyayeva, A., Herbener, S., Liu, E., Holdaway, D., and Johnson, B. T.: Data assimilation for the Model for Prediction Across Scales – Atmosphere with the Joint Effort for Data Assimilation Integration (JEDI-MPAS 1.0.0): EnVar implementation and evaluation, *Geosci. Model Dev.*, 15, 7859–7878, <https://doi.org/10.5194/gmd-15-7859-2022>, 2022.
- Kumar, R., Monache, L. D., Bresch, J., Saide, P. E., Tang, Y., Liu, Z., Silva, A. M. da, Alessandrini, S., Pfister, G., Edwards, D., Lee, P., and Djalalova, I.: Toward improving short-term predictions of fine particulate matter over the United States via assimilation of satellite aerosol optical depth retrievals, *J. Geophys. Res.-Atmos.*, 124, 2753–2773, <https://doi.org/10.1029/2018JD029009>, 2019.
- Mass, C. F., Ovens, D., Conrick, R., and Saltenberger, J.: The September 2020 wildfires over the Pacific Northwest, *Weather Forecast.*, 36, 1843–1865, <https://doi.org/10.1175/WAF-D-21-0028.1>, 2022.
- O'Dell, K., Ford, B., Fischer, E. V., and Pierce, J. R.: Contribution of wildland-fire smoke to US PM<sub>2.5</sub> and its influence on recent trends, *Environ. Sci. Technol.*, 53, 1797–1804, <https://doi.org/10.1021/acs.est.8b05430>, 2019.
- Pagowski, M., Grell, G. A., McKeen, S. A., Peckham, S. E., and Devenyi, D.: Three-dimensional variational data assimilation of ozone and fine particulate matter observations: some results using the Weather Research and Forecasting–Chemistry model and grid-point statistical interpolation, *Q. J. Roy. Meteor. Soc.*, 136, 2013–2024, <https://doi.org/10.1002/qj.700>, 2010.
- Pagowski, M., Liu, Z., Grell, G. A., Hu, M., Lin, H.-C., and Schwartz, C. S.: Implementation of aerosol assimilation in Grid-point Statistical Interpolation (v. 3.2) and WRF-Chem (v. 3.4.1), *Geosci. Model Dev.*, 7, 1621–1627, <https://doi.org/10.5194/gmd-7-1621-2014>, 2014.
- Park, S.-Y., Dash, U. K., Yu, J., Yumimoto, K., Uno, I., and Song, C. H.: Implementation of an ensemble Kalman filter in the Community Multiscale Air Quality model (CMAQ model v5.1) for data assimilation of ground-level PM<sub>2.5</sub>, *Geosci. Model Dev.*, 15, 2773–2790, <https://doi.org/10.5194/gmd-15-2773-2022>, 2022.
- Robichaud, A.: Surface data assimilation of chemical compounds over North America and its impact on air quality and Air Quality Health Index (AQHI) forecasts, *Air Qual. Atmos. Hlth.*, 10, 955–970, <https://doi.org/10.1007/s11869-017-0485-9>, 2017.
- Robichaud, A., Ménard, R., Zaitseva, Y., and Anselmo, D.: Multipollutant surface objective analyses and mapping of air quality health index over North America, *Air Qual. Atmos. Hlth.*, 9, 743–759, <https://doi.org/10.1007/s11869-015-0385-9>, 2016.
- Schwartz, C. S., Liu, Z., Lin, H.-C., and McKeen, S. A.: Simultaneous three-dimensional variational assimilation of surface fine particulate matter and MODIS aerosol optical depth, *J. Geophys. Res.-Atmos.*, 117, <https://doi.org/10.1029/2011JD017383>, 2012.
- Sluka, T.: Generic explicit diffusion operator added to JEDI, *JCSDA Quarterly Newsletter*, 74, <https://doi.org/10.25923/cfmw-2a05>, 2024.
- Sun, W., Liu, Z., Chen, D., Zhao, P., and Chen, M.: Development and application of the WRFDA-Chem three-dimensional variational (3DVAR) system: aiming to improve air quality forecasting and diagnose model deficiencies, *Atmos. Chem. Phys.*, 20, 9311–9329, <https://doi.org/10.5194/acp-20-9311-2020>, 2020.
- Tang, Y., Martin, C. R., Huang, M., Chai, T., Pagowski, M., Wang, H., Kleist, D. T., Baker, B., Campbell, P. C., Huang, J., McQueen, J. T., Montuoro, R., Tong, D., Stajner, I., Jung, Y., Kumar, R., and Kondragunta, S.: Develop and evaluate JEDI-based regional aerosol data assimilation for NOAA UFS-AQM system, The 103rd AMS Annual Meeting, Denver, Colorado, 2023.
- Trémolet, Y. and Auligné, T.: The Joint Effort for Data Assimilation Integration (JEDI), *JCSDA Quarterly Newsletter*, 66, 1–5, <https://doi.org/10.25923/RB19-0Q26>, 2020.
- Vogel, A., Ménard, R., Abu, J., and Chen, J.: Towards a parametric Kalman filter for operational wildfire plume assimilation: Formulation of the forecast step, *EGUsphere [preprint]*, <https://doi.org/10.5194/egusphere-2025-6386>, 2025.
- Wang, H., Weygandt, S., Pagowski, M., Li, R., Montuoro, R., Liu, Q., Dang, C., Ma, Y., Kumar, R., Kondragunta, S., Martin, C., Huang, J., McQueen, J., Stajner, I., and Hughes, B.: Assimilation of aerosol optical depth (AOD) retrievals and PM<sub>2.5</sub> in NCEP's next-generation regional air quality forecasting system, *WCRP-WWRP Symposium on Data Assimilation and Reanalysis*, 2021.
- Wang, H., Weygandt, S., Ahmadov, R., Li, R., Romero-Alvarez, J., Li, H., Grell, G., Pagowski, M., Tang, Y., Martin, C., McQueen, J., and Farooqui, M.: Assimilation of surface particulate matter observations in the experimental Rapid Refresh Forecast System coupled with smoke and dust model, *CU/CIRES Rendezvous 2023*, Boulder, Colorado, [https://insidecires.colorado.edu/rendezvous/uploads/Rendezvous\\_2023\\_7732\\_1683821981.pdf](https://insidecires.colorado.edu/rendezvous/uploads/Rendezvous_2023_7732_1683821981.pdf) (last access: 13 March 2026), 2023.
- Wang, H., Martin, C. R., Barré, J. E., Li, R., Allen, B., Luo, H., Weygandt, S. S., Hu, M., Ahmadov, R., Huang, J., Tang, Y., Choi, H., Tangborn, A., Wang, K., Liu, H., Stajner, I., Dang, C., Kondragunta, S., and Kumar, R.: Aerosol data assimilation within JEDI for NOAA's regional air quality model (AQM), *The 105th Annual Meeting of the American Meteorological Society*, New Orleans, Louisiana, 2025a.

- Wang, H., Martin, C., Barré, J., Li, R., Weygandt, S., Huang, J., Tang, Y., Choi, H., Wang, K., Liu, H., and Lee, J.: PM<sub>2.5</sub> assimilation within JEDI for NOAA's regional air quality model (AQMV7): application to the September 2020 western US wildfires, Zenodo [data set], <https://doi.org/10.5281/zenodo.17049857>, 2025b.
- Wei, Y., Zhao, X., Zhang, Z., Xu, J., Cheng, S., Liu, Z., Sun, W., Chen, X., Wang, Z., Hao, X., Li, J., and Chen, D.: Impact of model resolution and its representativeness consistency with observations on operational prediction of PM<sub>2.5</sub> with 3D-VAR data assimilation, *Atmos. Pollut. Res.*, 15, 102141, <https://doi.org/10.1016/j.apr.2024.102141>, 2024.
- Wen, J. and Burke, M.: Wildfire smoke plume segmentation using geostationary satellite imagery, arXiv, <https://doi.org/10.48550/arXiv.2109.01637>, 2021.
- Wu, J.-B., Xu, J., Pagowski, M., Geng, F., Gu, S., Zhou, G., Xie, Y., and Yu, Z.: Modeling study of a severe aerosol pollution event in December 2013 over Shanghai, China: An application of chemical data assimilation, *Particuology*, 2015, <https://doi.org/10.1016/j.partic.2014.10.008>, 2015.
- White, S. R., Sugrue, R. A., Guillotte, L., James, E., Wang, H., Ahmadov, R., Thakur, N., and Chow, F. K.: Hourly PM<sub>2.5</sub> estimates across California from 2018 to 2023, *ACS ES&T Air*, <https://doi.org/10.1021/acsestair.5c00372>, 2026.
- Zhang, H., Yee, L. D., Lee, B. H., Curtis, M. P., Worton, D. R., Isaacman-VanWertz, G., Offenberg, J. H., Lewandowski, M., Kleindienst, T. E., Beaver, M. R., Holder, A. L., Lonnenman, W. A., Docherty, K. S., Jaoui, M., Pye, H. O. T., Hu, W., Day, D. A., Campuzano-Jost, P., Jimenez, J. L., Guo, H., Weber, R. J., de Gouw, J., Koss, A. R., Edgerton, E. S., Brune, W., Mohr, C., Lopez-Hilfiker, F. D., Lutz, A., Kreisberg, N. M., Spielman, S. R., Hering, S. V., Wilson, K. R., Thornton, J. A., and Goldstein, A. H.: Monoterpenes are the largest source of summertime organic aerosol in the southeastern United States, *P. Natl. Acad. Sci. USA*, 115, 2038–2043, <https://doi.org/10.1073/pnas.1717513115>, 2018.